

This work was written as part of one of the author's official duties as an Employee of the United States Government and is therefore a work of the United States Government. In accordance with 17 U.S.C. 105, no copyright protection is available for such works under U.S. Law.

Public Domain Mark 1.0

<https://creativecommons.org/publicdomain/mark/1.0/>

Access to this work was provided by the University of Maryland, Baltimore County (UMBC) ScholarWorks@UMBC digital repository on the Maryland Shared Open Access (MD-SOAR) platform.

Please provide feedback

Please support the ScholarWorks@UMBC repository by emailing scholarworks-group@umbc.edu and telling us what having access to this work means to you and why it's important to you. Thank you.

EVALUATION OF EMISSION MECHANISMS AT ω_{pe} USING *ULYSSES* OBSERVATIONS OF TYPE III BURSTS

G. THEJAPPA¹ AND D. LENGYEL-FREY

Department of Astronomy, University of Maryland, College Park, MD 20742

AND

R. G. STONE AND M. L. GOLDSTEIN

NASA, Goddard Space Flight Center, Greenbelt, MD 20771

Received 1992 November 6; accepted 1993 April 27

ABSTRACT

We present the first observational tests of existing theories for the generation of type III radio bursts emitting at the fundamental plasma frequency, ω_{pe} . This study is based on local radio emission and in situ wave phenomena associated with four interplanetary type III radio bursts observed by the unified radio and plasma wave experiment on the *Ulysses* spacecraft. Intense Langmuir wave peaks with energy densities and rapid time variations indicative of Langmuir solitons are observed for some events. Low-frequency waves below 500 Hz are not observed. For each event, brightness temperatures derived from radio observations are compared with those predicted by various mechanisms for the conversion of Langmuir waves to electromagnetic radiation. The theories tested here are: (1) scattering of Langmuir waves by thermal ions; (2) wave-wave interactions, i.e., merging and decay processes involving Langmuir and low-frequency waves; (3) strong turbulence phenomena involving Langmuir solitons; and (4) direct coupling between Langmuir and electromagnetic waves due to density gradients. The mechanism of scattering on thermal ions may be ruled out as a major source of electromagnetic radiation since it yields brightness temperatures well below observed type III values. Wave-wave interactions yield brightness temperatures four to six orders of magnitude greater than observed values. The strong turbulence mechanism and the direct coupling mechanism predict brightness temperatures less than two orders of magnitude too large.

Subject headings: interplanetary medium — radiation mechanisms: miscellaneous — solar wind — Sun: radio radiation

1. INTRODUCTION

The purpose of this study is to determine what mechanism or mechanisms may be responsible for generating interplanetary type III radio bursts at the fundamental plasma frequency. The type III radio burst phenomenon involves the excitation of Langmuir waves by electron beams and the conversion of Langmuir waves into escaping radiation at ω_{pe} and $2\omega_{pe}$, where ω_{pe} is the plasma frequency. Although past studies have focused on problems of stabilizing the electron beam responsible for the type III emission, there has been no systematic study of the processes by which Langmuir waves are converted into electromagnetic radiation at ω_{pe} and $2\omega_{pe}$. Conversion processes for producing $2\omega_{pe}$ radiation have been evaluated by Gurnett et al. (1980) who, assuming type III bursts emit at $2\omega_{pe}$, used observed interplanetary type III emissivities (Tokar & Gurnett 1980) and associated Langmuir fluxes to evaluate the incoherent induced scattering mechanism (Smith 1977) and the coherent parametric (oscillating two-stream) mechanism (Papadopoulos, Goldstein, & Smith 1974). They found overall agreement of both mechanisms with observations, even though the absolute emissivity tended to favor the incoherent process when compared with the somewhat idealized model of Papadopoulos et al. (1974).

Conversion mechanisms for producing type III radiation at ω_{pe} have not been tested observationally. This may be due in part to the long-standing controversy about whether interplanetary type III emission occurs at ω_{pe} . Early studies of these bursts tended to favor the $2\omega_{pe}$ interpretation (Fainberg,

Evans, & Stone 1972; Fainberg & Stone 1974), although later work found evidence for both ω_{pe} and $2\omega_{pe}$ emission (Dulk, Steinberg, & Hoang 1984; Kellogg 1986). Recently, Reiner, Fainberg, & Stone (1992) have identified several interplanetary type III bursts with emission at both ω_{pe} and $2\omega_{pe}$ and with associated Langmuir wave activity.

There are at least four known mechanisms for the conversion of Langmuir waves into electromagnetic waves at ω_{pe} . They are (1) wave-particle interactions involving both spontaneous and induced scattering of Langmuir waves into electromagnetic radiation by thermal ions (Ginzburg & Zheleznyakov 1958; Smith 1970; Melrose 1974, 1977; Zaitsev 1975, 1977); (2) wave-wave interactions involving either merging of Langmuir waves with low frequency waves to produce electromagnetic waves or, alternatively, the decay of Langmuir waves into low-frequency and electromagnetic waves (Takakura 1979; Melrose 1980a, 1989; Melrose, Dulk, & Cairns 1986; Lin et al. 1986; Cairns 1987); (3) strong turbulence involving emission of electromagnetic waves by a Langmuir soliton (Goldman, Reiter, & Nicholson 1980) or incoherent emission due to scattering of long-wavelength Langmuir waves on collapsed Langmuir cavitons (Kruchina, Sagdeeva, & Shapiro 1980); and (4) direct coupling between Langmuir and electromagnetic waves due to large-scale gradients or local inhomogeneities in the electron density (Field 1956; Zheleznyakov 1970; Melrose 1980b).

This study is based on observations of type III bursts with emission at ω_{pe} and with associated Langmuir wave activity. To identify the conversion mechanisms which produce fundamental plasma emission in interplanetary type III bursts, we

¹ On leave from Indian Institute of Astrophysics, Bangalore 560034, India.

derive the brightness temperatures (T_B) of type III bursts by using the observed Langmuir wave energy densities in each of the above-mentioned mechanisms and compare the derived with the observed T_B values of the associated type III bursts. In § 2 we present the unified radio and plasma wave (URAP) observations of the various wave phenomena upon which this study is based. In § 3, the effective temperatures of electromagnetic waves, Langmuir waves and ion-acoustic waves are obtained from electric field observations. The Langmuir wave effective temperatures are used in § 4 to compute type III brightness temperatures predicted by each theoretical model. The effective temperatures of the electromagnetic waves, i.e., the brightness temperatures of the type III radio bursts, are used for comparison with the theoretical predictions. In § 5 we discuss the results of the model predictions in light of type III observations to determine the feasibility of each conversion mechanism. In § 6 we present the summary and conclusions. Finally, we note that in order to do a meaningful comparison of brightness temperatures predicted by the various models, we must use a standard set of those physical parameters which are common to the models. These parameters are listed in Table 1 and have been selected to represent typical solar wind plasma conditions.

2. OBSERVATIONS

The URAP experiment (Stone et al. 1992) on board the *Ulysses* spacecraft is uniquely suited to study questions concerning the generation of type III radio bursts. The experiment consists of a radio receiver to study electromagnetic waves propagating to the spacecraft from remote regions, as well as a number of instruments which record in situ plasma waves generated at the spacecraft. Data from four of the URAP instruments are pertinent to this study: the radio astronomy receiver (RAR), plasma frequency receiver (PFR), wave form analyzer (WFA), and fast envelope sampler (FES).

1. *Radio astronomy receiver (RAR).*—The RAR measures electric field signals over the frequency range of 1–940 kHz. At frequencies above the local plasma frequency, electromagnetic waves from solar radio bursts are detected, which propagate to the spacecraft from remote regions of the interplanetary medium. The RAR is also sensitive to the electrostatic quasi-thermal noise continuum, caused by the coupling of the antenna to the local plasma. The low-frequency cutoff of this continuum, referred to as the plasma line, occurs at the local plasma frequency and therefore provides an accurate measurement of the electron density at the spacecraft. The frequency resolution below 50 kHz is essentially continuous, with frequency spacings of 0.75 kHz and bandwidths of 0.75 kHz for each frequency channel. Frequencies below 50 kHz are sampled every 128 s.

2. *Plasma frequency receiver (PFR).*—The PFR measures the electric field between 0.5 and 35 kHz in 32 logarithmic frequency steps, with a 14% spacing between frequencies and a bandwidth of about 14% of the center frequency. The highest time resolution of the data is 16 s.

3. *Wave form analyzer (WFA).*—The WFA provides on-board spectral analysis of signals from both electric and magnetic field preamplifiers, yielding spectral data for 24 frequencies in the 0.08 to 448 Hz range, with a bandwidth of 30% of the center frequency. The time resolution is 64 s for the highest bit rate.

4. *Fast envelope sampler (FES).*—The FES records intense plasma wave activity with a time resolution of up to 1 ms per

data sample, and a total of 1024 contiguous samples recorded for an event. The most intense event observed during an interval of approximately one-half hour is telemetered. Electric field measurements are made over a wide-frequency band determined by commandable filters, each having a range of one decade in frequency, e.g., 6–60 kHz.

In a recent study, three interplanetary type III radio bursts observed by the *Ulysses* URAP experiment were found to have emission near the local plasma frequency ω_{pe} and its harmonic and to be associated with Langmuir wave activity at the same frequency (Reiner et al. 1992). The value of ω_{pe} was determined from the plasma line as observed by the RAR during the time of each type III event. These type III bursts are unique in that the peak of the ω_{pe} and $2\omega_{pe}$ emission does not drift to lower frequencies with time, as opposed to type III bursts observed at higher frequencies. The emission of these nondrifting bursts is therefore referred to as “local” emission, whereas bursts at higher frequencies are “remote” type III bursts. Three such events occurred on 1990 December 11, 1990 December 23 and 1991 February 22. We have identified a fourth event with type III emission and Langmuir wave activity near ω_{pe} . This event occurred on 1991 March 7. This event is included in the present analysis due to the simultaneous occurrence of electromagnetic and Langmuir wave emissions approximately at the same frequency. These four events form the observational basis of the current study.

In Figure 1, we present the in situ observations of the type III solar radio burst and other wave activity observed on 1990 December 11. Figure 1a represents peak RAR data during each 128 s observing interval. Figures 1b and 1c display peak PFR

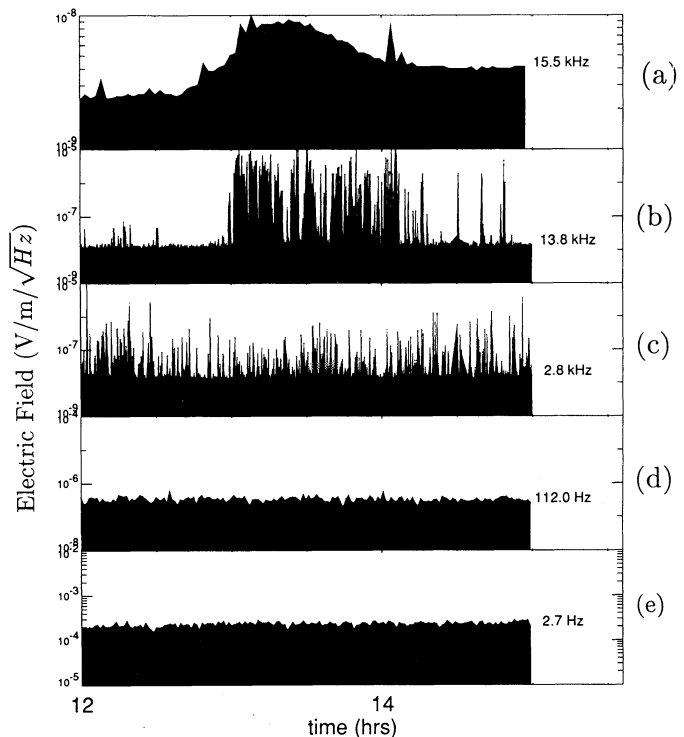


FIG. 1.—Radio wave and in situ plasma wave phenomena observed on 1990 December 11: (a) type III radio emission observed by the RAR at 15.5 kHz; (b) Langmuir waves observed by the PFR; (c) PFR observations of the high-frequency ion acoustic waves; (d)–(e) WFA observations. No wave activity is apparent at these frequencies.

data for 16 s intervals, whereas Figures 1d and 1e represent 64 s average WFA data. The smoothly varying emission in Figure 1a beginning before 13:00 UT is a type III radio burst with a peak of $\approx 10^{-8} \text{ V m}^{-1} \text{ Hz}^{-1/2}$ in the observed electric field. Figure 1b displays the sporadic bursts of Langmuir waves observed at 13.8 kHz by the PFR. Langmuir wave peak electric field strengths are up to 1000 times more intense than the peak in the observed type III burst electric field.

The spectral evolution of the type III burst is shown in Figure 2, where the electric field signals recorded by the closely spaced channels of the RAR from 12.5 to 15.5 kHz are displayed. The irregular peaks seen from 12.5 to 14.8 kHz are Langmuir waves which peak in intensity in the 13.3 kHz channel. It is known from the frequency of the plasma line as observed by the RAR that the plasma frequency during this period was 13.6 kHz (Reiner et al. 1992). The lower envelopes of the Langmuir peaks reflect the smooth variation of the electric field, which is characteristic of type III bursts. There is a gradual transition from profiles at lower frequencies dominated by Langmuir waves to those at higher frequencies displaying only fundamental type III emission.

Langmuir waves are inherently "bursty" in nature, and therefore, their observed peak intensities depend on the time resolution of the observations. Usually peak intensities derived from PFR observations are greater than those obtained from the lower time resolution RAR data. Even larger Langmuir wave electric field strengths are obtained from the FES due to its millisecond sampling rate. Figure 3 shows three FES events which correspond to Langmuir bursts occurring at 13:02 UT,

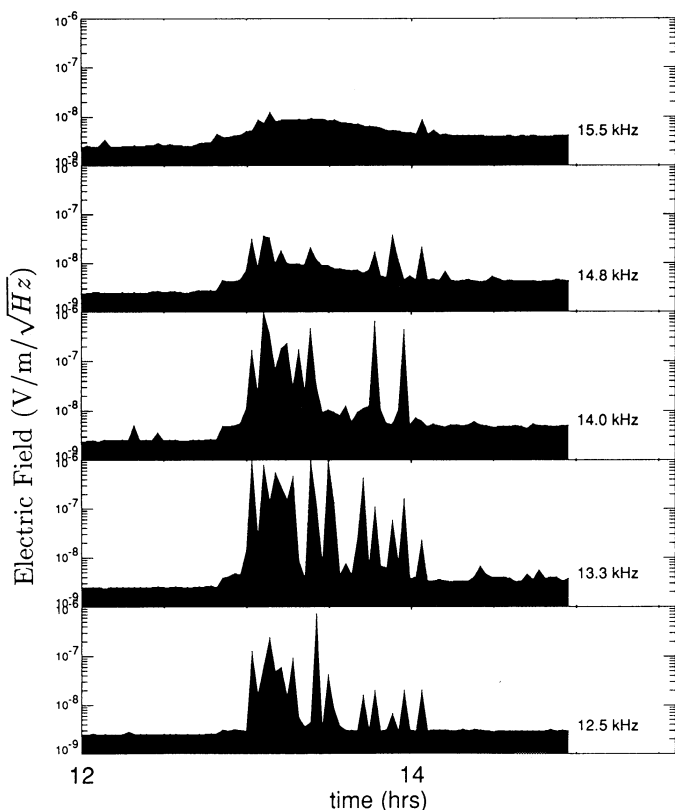


FIG. 2.—Intensity of electric fields observed by different channels of the RAR for the type III burst observed on 1990 December 11. The transition from spiky Langmuir waves, which peak at 13.3 kHz, to the smooth type III radio burst, which predominates below about 15.5 kHz, is shown.

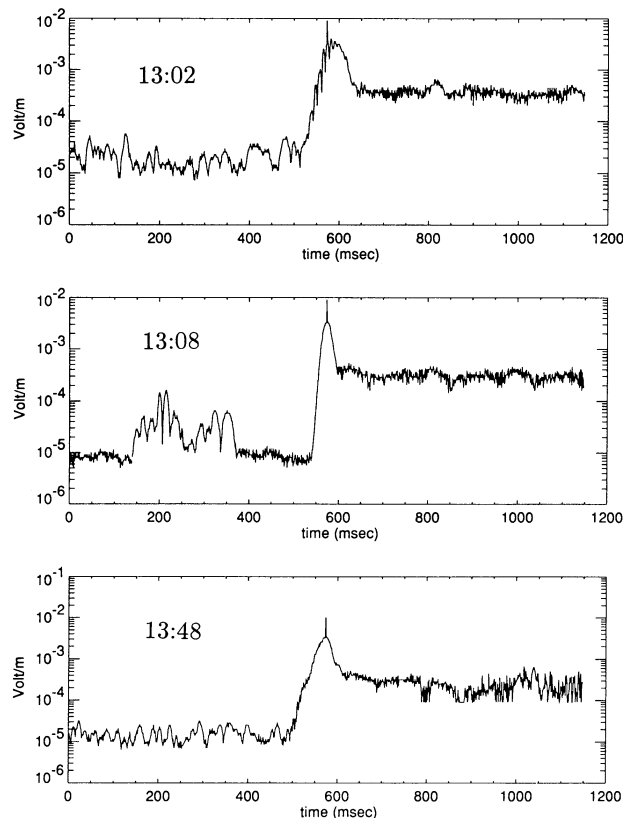


FIG. 3.—High time resolution observations of Langmuir waves observed by the FES during the 1990 December 11 type III burst. The times of the three FES events are given. The spikes occurring at the peak of each event may correspond to a Langmuir soliton. The 6–60 kHz band and 1.12 ms time resolution were used. The enhanced background level after about 600 ms in each panel is caused by the switch-on of the 32 dB attenuator.

13:08 UT, and 13:48 UT. The time resolution of the FES data is 1.12 ms, and each event is observed for approximately 1 s. The frequency band for these observations covers 6–60 kHz. During each of the three events a 32 dB attenuator is activated soon after the event peak at about 600 ms and remains on for the duration of the event. Complex structures occur during these events, and emission peaks with intensities approaching 10 mV m^{-1} are observed. Similar intensities have been found in FES observations of the other events of this study. Such large peak intensities indicate that strong turbulence effects are important for these events and may play a role in the Langmuir wave conversion process. This is discussed further in §§ 4 and 5.

Figure 1c prominently displays high-frequency ion-acoustic waves (Gurnett & Frank 1978) observed by the PFR at 2.8 kHz. The wave activity in this frequency range appears to be well developed and very intense. The presence of these waves is of interest because Lin et al. (1986) have stated that these waves generally do not occur during intervals of type III-associated Langmuir waves. We present in Figure 4a Langmuir wave activity from PFR observations integrated over approximately 10–15 kHz. Figure 4b shows PFR observations of high-frequency ion-acoustic waves integrated over the range of 1 to 5 kHz. It is clear that this high-frequency ion-acoustic wave activity is intense during the Langmuir activity. However, as we will demonstrate in § 5, it is unlikely that these waves participate in wave-wave conversion processes, because they do

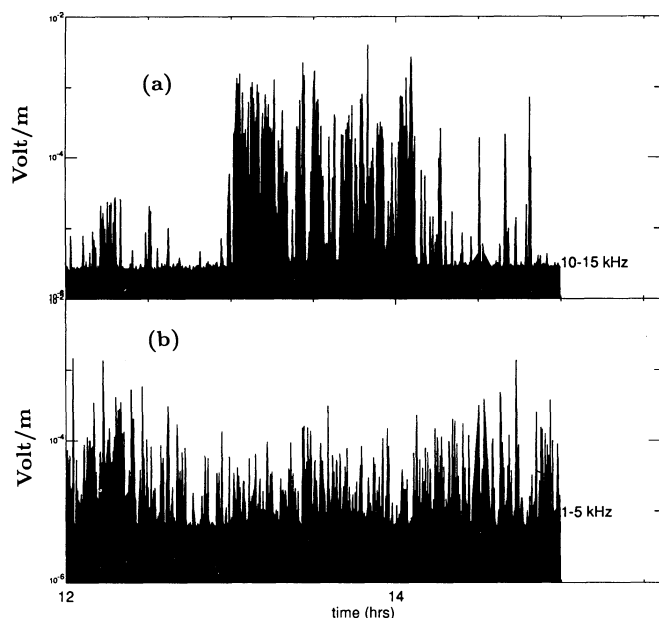


FIG. 4.—PFR time profiles for the 1990 December 11 event integrated over frequency: (a) integration from 10 to 15 kHz; (b) integration from 1 to 5 kHz.

not satisfy the resonance conditions for interactions with Langmuir waves.

In the WFA data shown in Figures 1d and 1e, no wave activity is apparent either at 112 Hz or 2.7 Hz. A similar scarcity of observed waves in this frequency range has been found for the other three events of this study. The absence of any wave activity near 100 Hz contradicts the finding of Lin et al. (1986) that type III bursts with accompanying Langmuir wave activity are most often associated with waves near 100 Hz, which they refer to as long-wavelength ion-acoustic waves. The question of whether these low-frequency ion-acoustic waves are present or not is important, since Lin et al. (1986) have suggested that the decay of Langmuir waves into low-frequency ion-acoustic waves and electromagnetic waves may explain type III emission at ω_{pe} . Indeed, wave activity near 100 Hz does satisfy the resonance conditions for wave-wave interactions involving Langmuir waves and therefore could produce electromagnetic waves through nonlinear wave-wave interactions. The presence or absence of waves at 2.7 Hz also has strong implications for strong turbulence theories, such as those involving the oscillating two-stream instability. This will be discussed further in §§ 4 and 5.

Figure 5 shows spectral data from the RAR, PFR, and WFA instruments during the peak of the 1990 December 11 type III event, from approximately 13:10 to 13:15 UT. There are two prominent peaks in Figure 5a, the first one corresponding to Langmuir waves at about 13.5 kHz and the second broader peak at about 40 kHz corresponding to type III emission from remote regions. The “local” type III fundamental emission is almost completely masked by the Langmuir wave activity, indicating that the Langmuir wave spectral power is vastly greater than that of the “local” type III emission. These sharp spectral peaks near 13.5 kHz in both Figures 5a and 5b reflect the narrow-banded nature of the beam-excited Langmuir waves. The weak spectral peaks seen below 10 kHz in both figures are due to high-frequency ion-acoustic waves. As shown in Figure 5c, no wave activity is observed by the WFA above the instrumental threshold at frequencies below about 500 Hz.

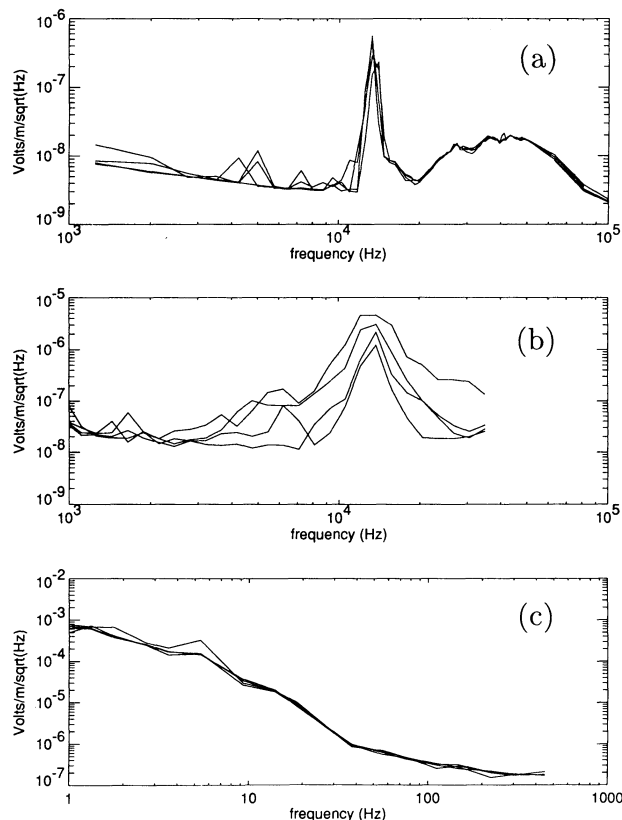


FIG. 5.—Selected electric field spectra observed between 13:10 and 13:15 UT on 1990 December 11: (a) RAR observations; (b) PFR observations; (c) WFA observations.

The dominance of the Langmuir wave energy relative to that in type III emission is shown more clearly in Figure 6, where RAR observations of Langmuir waves and the type III burst are superposed. The Langmuir wave profile is integrated over the frequency range from 11 to 14 kHz, while the type III emission is integrated from 15 to 18 kHz. It is clear that only a small fraction of Langmuir wave energy is converted into electromagnetic waves.

In Figure 7, we present the wave activity observed during the type III event of 1990 December 23. Using the frequency of the plasma line we estimate that the plasma frequency during the

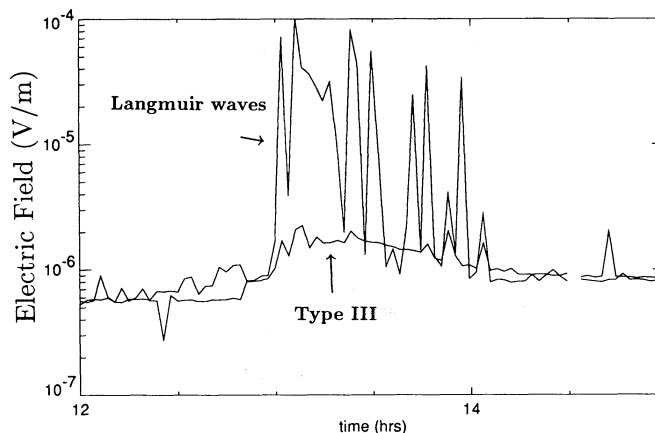


FIG. 6.—Superposition of the Langmuir wave bursts from 11 to 14 kHz on the smoothly varying type III burst profile from 15 to 18 kHz for the 1990 December 11 event.

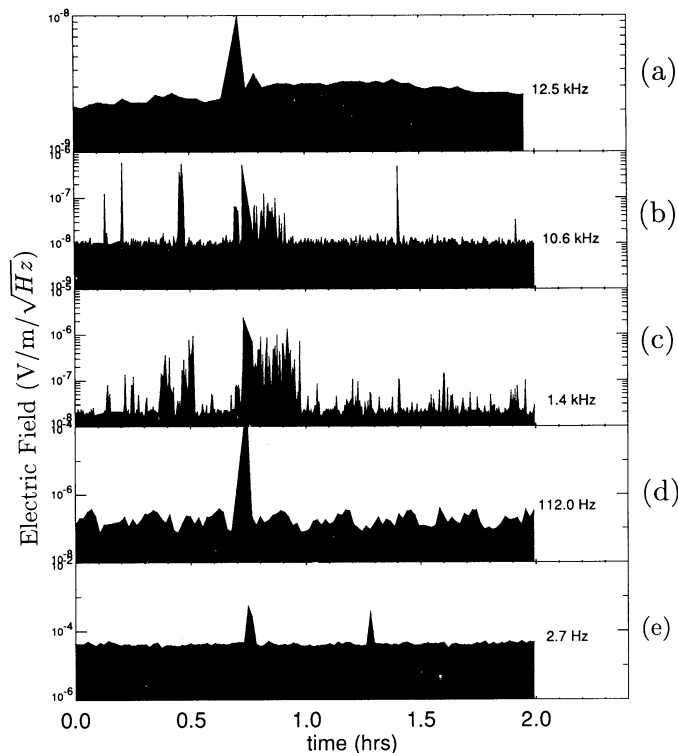


FIG. 7.—Type III burst and associated wave activity observed on 1990 December 23. The intensity peak at about 00:40 UT is due to instrumental calibration. (a) RAR observations; (b)–(c) PFR observations; (d)–(e) WFA observations.

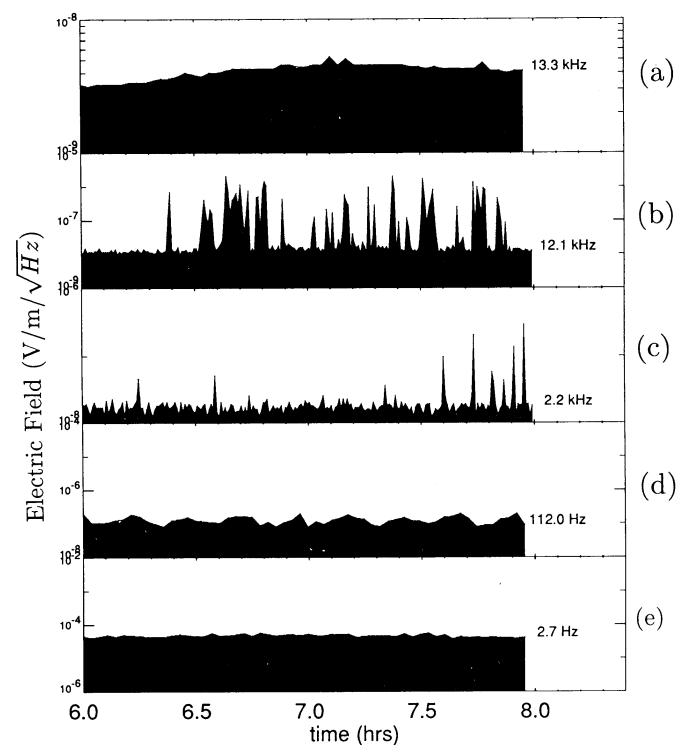


FIG. 8.—Type III burst and associated wave activity observed on 1991 February 22: (a) RAR observations; (b)–(c) PFR observations; (d)–(e) WFA observations.

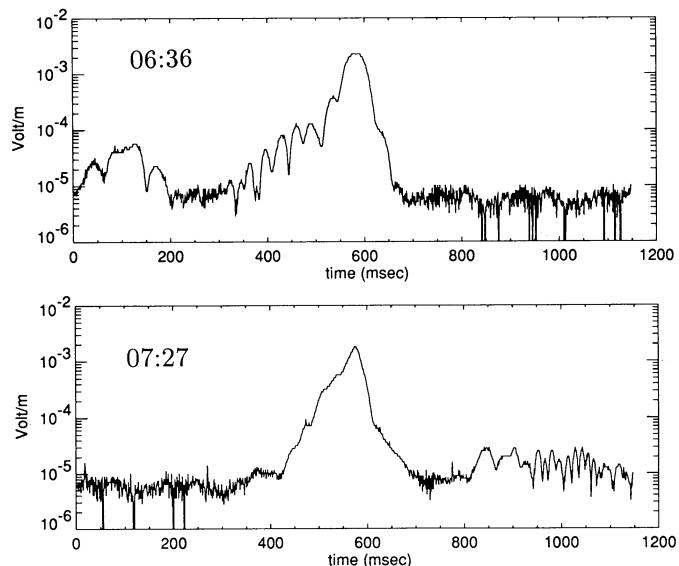


FIG. 9.—FES events observed during 1991 February 22 type III burst. For these events, no emission spikes are evident, implying that no Langmuir solitons are present.

peak of this event is ≈ 9.7 kHz. The prominent peak seen at about 00:40 UT in all panels in Figure 7 is due to instrument calibration. No FES events were observed during the 1990 December 23 burst, since the associated Langmuir activity was very weak. Indeed, high-frequency ion-acoustic waves observed at 1.4 kHz show greater intensities than the Langmuir waves during this interval. The variation in the background level seen at 112 Hz frequency is due to instrumental

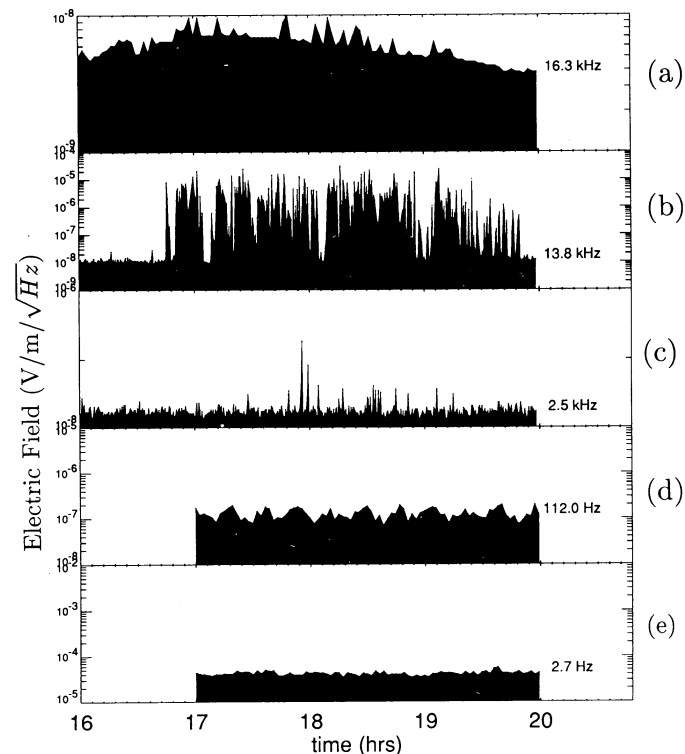


FIG. 10.—Type III burst and associated wave activity observed on 1991 March 7: (a) RAR observations; (b)–(c) PFR observations; (d)–(e) WFA observations.

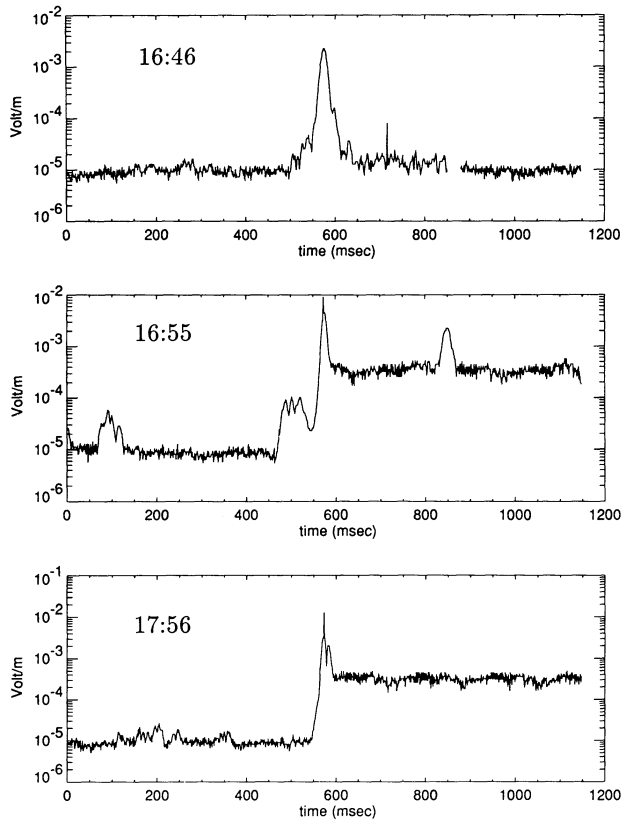


FIG. 11.—FES events corresponding to the Langmuir waves observed during 1991 March 7 type III event.

interference. Neither at 112 Hz nor in the 2.7 Hz is there any evidence of wave activity.

Figure 8 shows the wave activity observed during the type III event of 1991 February 22. We estimate the plasma frequency to be ≈ 10.6 kHz during this event. Once again there is no evidence of wave activity either at 112 Hz or at 2.7 Hz. The FES recorded strong Langmuir events at 06:36 UT and 07:27 UT. These are shown in Figure 9. Unlike the FES events of 1990 December 11 (Fig. 3), these events do not show intense spikes at the event peaks and are therefore somewhat weaker than the December 11 FES events.

The type III event of 1991 March 7 is presented in Figure 10 with its associated wave activity. We have estimated the plasma frequency during this event to be ≈ 14.8 kHz. The background fluctuations seen at 112 Hz are again due to instrumental interference. The FES observations of the Langmuir wave bursts are presented in Figure 11.

In the following section we give the formulae for computing the effective temperatures of the waves analyzed in this study, specifically electromagnetic, Langmuir, and ion-acoustic waves.

3. EFFECTIVE TEMPERATURES OF ELECTROMAGNETIC, LANGMUIR, AND ION-ACOUSTIC WAVES

The effective temperature T_{eff} and total energy density W are related by

$$T_{\text{eff}} = \frac{(2\pi)^3 W}{k^2 \Delta k \Omega} \quad (1)$$

(see Zheleznyakov 1977), where k and Δk are the wavenumber and wavenumber range, respectively, and Ω is the solid angle of the source. The energy density W is related to the electric field E by

$$W = \epsilon_0 E^2 \quad (2)$$

(Melrose 1986), for both electromagnetic and Langmuir waves, whereas for ion-acoustic waves it is given by

$$W = \frac{\epsilon_0 E^2}{(k_s \lambda_D)^2}, \quad (3)$$

where ϵ_0 is the dielectric permittivity of free space, k_s is the wavenumber of the ion-acoustic waves, and λ_D is the Debye length. The standard set of physical parameters adopted in the present study are listed in Table 1. These parameters represent typical plasma conditions in the interplanetary medium.

3.1. Local Type III Radio Emission

By using the dispersion relation for electromagnetic waves in a plasma $\omega^2 = (\omega_{pe}^2 + k^2 c^2)$ we can write $k = 2\pi f n_t / c$. Here c is the speed of light, $f = \omega/2\pi$ is the observing frequency of the electromagnetic waves, f_{pe} is the plasma frequency, and $n_t = \sqrt{1 - f_{pe}^2/f^2}$ is the refractive index of electromagnetic waves. By differentiating the dispersion relation we obtain the spread in the wavenumbers as $\Delta k = 2\pi \Delta f / n_t c$, where Δf is the receiver bandwidth. By substituting equation (2) in equation (1), we obtain:

$$T_B = 1.73 \times 10^{37} \frac{E_t^2}{n_t f^2 \Omega_t}, \quad (4)$$

where T_B is the effective temperature of the electromagnetic radiation, usually referred to as the brightness temperature, in kelvins, f is in hertz, and E_t is the electric field in units of $\text{V m}^{-1} \text{Hz}^{-1/2}$. The solid angle Ω_t of the type III source is given by

$$\Omega_t = 2\pi(1 - \cos \theta), \quad (5)$$

where θ is its angular radius. Here one should note that the formula given in equation (4) coincides exactly with the formula given by Steinberg & Hoang (1986), who use $n_t \approx 1$ and the relation $T_A \Omega_A = T_B \Omega_t$, where $\Omega_A = 8\pi/3$ is the antenna effective beam solid angle in steradians and T_A is the antenna temperature. The observed voltage V and T_A are related by Nyquist's theorem $V^2 = 4\kappa T_A R_A$, where κ is the Boltzmann constant and R_A is the antenna radiation resistance, which is related to the antenna length L_A by $R_A = 80\pi^2 L_A^2 f^2 c^{-2}$.

It was reported by Steinberg et al. (1984, 1985) that at low observing frequencies, i.e., $f \leq 60$ kHz, the angular radii (θ) of type III sources saturate at about 90° , which implies $\Omega_t \approx 2\pi$. Therefore, equation (4) gives $T_B = 2.8 \times 10^{36} E_t^2 / f^2 n_t$, which is used to calculate the observed brightness temperatures T_B of the local type III emission from the electric field strengths E_t observed by the RAR at the peak of the radio emission. Table 2 presents the type III observations used in this analysis. Column (1) gives the event date, column (2) gives the plasma frequency during each event, column (3) lists the frequency at which the most intense type III emission was observed, column (4) gives the electric field strength at the peak of the type III burst, column (5) lists the brightness temperature derived from E_t , and the last column shows the heliocentric distance of the *Ulysses* spacecraft at the time of each event.

TABLE 1
VALUES OF PLASMA, BEAM AND WAVE PARAMETERS USED IN THE ANALYSIS

Parameter	Value
Electron density, n_e	2 cm^{-3}
Electron temperature, T_e	$2 \times 10^5 \text{ K}$
Ion temperature, T_i	$4 \times 10^4 \text{ K}$
Debye length, λ_D	$2.2 \times 10^3 \text{ cm}$
Electron plasma frequency, f_{pe}	13 kHz
Electron thermal velocity, v_{Te}	$1.7 \times 10^8 \text{ cm s}^{-1}$
The scale length of density variation, $L_n = n_e/\nabla n_e \simeq$	0.5 AU
The size of the emitting system, L	$3 \times 10^{10} \text{ cm}$
Solar wind velocity, v_{sw}	400 km s^{-1}
Ion plasma frequency, f_{pi}	300 Hz
Beam velocity, v_b	$3.5 \times 10^9 \text{ cm s}^{-1}$
Beam width, $\Delta v_b/v_b$	$\simeq 0.15$
Beam excited Langmuir wave number, k_L	$2.3 \times 10^{-5} \text{ cm}^{-1}$
The spread in wavenumbers, Δk_L	$\simeq 0.15 k_L$
Langmuir wave phase velocity, $v_{ph} \simeq v_b$	$3.5 \times 10^9 \text{ cm s}^{-1}$
The group velocity of EM waves, v_g	$0.5c$
Typical ion-acoustic wave number, k_s	$\simeq k_L$
Ion-acoustic speed, c_s	$5.2 \times 10^6 \text{ cm s}^{-1}$
Ion-acoustic frequency, $\omega_i/2\pi$	19 Hz
Instrumental threshold at 100 Hz	$2.5 \times 10^{-6} \text{ V m}^{-1}$
Type III source size, Ω_i	2π
Langmuir wave source size, $\Omega_L \simeq 4\Delta v_b/v_b$	0.6π
Ion-acoustic source size, Ω_s	$\simeq \Omega_L$
Amplitude of Langmuir spike, $E_{L\text{spike}}$	12.8 mV m^{-1}

3.2. Langmuir Waves

We compute the effective temperature of Langmuir waves T_L using the electric field strengths E_L observed by the FES for each event. The electric field strengths have been determined from FES data, as shown in Figures 3, 9, and 11. In these plots a broad intensity peak occurs near the midpoint of the plot, and in some cases a sharp spike with an intensity of about 10^{-2} V m^{-1} is superposed on the broader peak (see, for example, Fig. 3). As will be discussed in § 4.3, the spikes are likely to be signatures of Langmuir solitons, whereas the broader under-

TABLE 2

TYPE III BURST OBSERVATIONS FROM RAR MEASUREMENTS

Event (1)	f_{pe} (kHz) (2)	f (kHz) (3)	E_t ($\text{V m}^{-1} \text{ Hz}^{-1/2}$) (4)	T_B (K) (5)	R (AU) (6)
1990 Dec 11	13.6	15.5	1×10^{-8}	2×10^{12}	1.35
1990 Dec 23	9.7	12.5	4×10^{-9}	5×10^{11}	1.46
1991 Feb 22	10.6	13.3	3×10^{-9}	2×10^{11}	2.12
1991 Mar 7	14.8	16.3	5×10^{-9}	6×10^{11}	2.34

NOTE.—Col. (1) gives date of type III event; col. (2), the plasma frequency; col. (3), the frequency of the most intense type III emission; col. (4), the electric field strength of electromagnetic waves at peak of type III burst; col. (5), the observed type III brightness temperature derived from E_t ; and col. (6), the heliocentric distance of *Ulysses* spacecraft.

TABLE 3

LANGMUIR WAVE OBSERVATION FROM FES EVENT DATA

EVENT (1)	E_L (V m^{-1})				$W_L/n_e T_e$ (6)	T_L (K) (7)
	(2)	(3)	(4)	(5)		
1990 Dec 11	4×10^{-3}	4×10^{-3}	4×10^{-3}	...	2×10^{-5}	7×10^{17}
1990 Dec 23
1991 Feb 22	2×10^{-3}	2×10^{-3}	1×10^{-5}	2×10^{17}
1991 Mar 7	2×10^{-3}	5×10^{-3}	4×10^{-3}	4×10^{-3}	3×10^{-5}	1×10^{18}

NOTE.—Col. (1) gives the date of type III event; cols. (2–5), the electric field strength of Langmuir waves for each FES event; col. (6), the Langmuir wave energy density based on maximum E_L value of each FES event; and col. (7), the Langmuir wave effective temperature from maximum E_L value.

lying peaks represent longer wavelength Langmuir waves. Since not all FES events display the spike features, and since more spectral power is contained in the broad peaks than in the spikes, we determine E_L from the maximum of the broad peak for each FES event.

As we have discussed, the FES filters have a very wide-band response, e.g., 6–60 kHz at the higher frequencies. However, as shown in the RAR and PFR measurements in Figure 5, the total power in Langmuir waves is confined to a very narrow frequency range. Therefore, FES measurements do not provide a meaningful determination of the Langmuir electric field in $\text{V m}^{-1} \text{ Hz}^{-1/2}$, the units used in equation (4). As a consequence, we use equation (1) to calculate T_L , which is then:

$$T_L = 8.7 \times 10^{22} \frac{E_L^2}{\Omega_L} \quad (6)$$

Following Lin et al. (1986), we have used $k_L \simeq 2.3 \times 10^{-5} \text{ cm}^{-1}$ and $\Delta k_L/k_L \simeq \Delta v_b/v_b \simeq 0.15$, where v_b and Δv_b are the velocity and velocity spread of the energetic beam electrons, respectively. The Langmuir waves emitted at an angle $\theta \leq 1$ with respect to the beam velocity propagate in a solid angle $\Omega_L \simeq 4\pi\Delta v_b/v_b \simeq 0.6\pi$ (Ginzburg & Zheleznyakov 1958), yielding $T_L \simeq 4.6 \times 10^{22} E_L^2$.

Table 3 presents the Langmuir wave observations used in this analysis. Columns (2) through (5) give electric field strengths of the broad emission peak from each FES event observed during a type III burst. The most intense field strength for each burst is used to compute values in columns (6) and (7). Column (6) of Table 3 gives the normalized Langmuir wave energy density, based on measured n_e values and using T_e values from Table 1, and column (7) gives the Langmuir wave effective temperature.

3.3. Ion-Acoustic Waves

The effective temperature of ion-acoustic waves (T_s) is calculated using equations (1) and (3). Using parameters given in Table 1 we obtain:

$$T_s \simeq 3.4 \times 10^{25} \frac{E_s^2}{\Omega_s}, \quad (7)$$

where the electric field E_s is in units of V m^{-1} and Ω_s is the solid angle of the ion-acoustic source. For $\Omega_s \simeq \Omega_L \simeq 0.6\pi$, we obtain $T_s \simeq 1.8 \times 10^{25} E_s^2$.

We next proceed to compute brightness temperatures of type III bursts predicted by each conversion mechanism.

4. CALCULATIONS OF BRIGHTNESS TEMPERATURE FROM CONVERSION MECHANISMS

The conversion of Langmuir waves into electromagnetic waves through various nonlinear plasma processes for steady

state conditions can be described by the transfer equation for the brightness temperature T_B :

$$\frac{\partial T_B}{\partial l} = \alpha - \mu T_B, \quad (8)$$

where l is the radiation path length. Here the emission coefficient α describes spontaneous emission processes, and the absorption coefficient μ describes damping when it is positive and induced emission processes when it is negative. The solution of the transfer equation (8) for the case of $\mu > 0$ can be written as:

$$T_B = \frac{\alpha}{\mu} [1 - \exp(-\mu L)], \quad (9)$$

where L is the linear dimension of the source. This yields $T_B \approx \alpha/\mu$ for optical depth $\mu L \gg 1$; alternatively, $T_B \approx \alpha L$ for $\mu L \ll 1$. For the case of $\mu < 0$, the solution of the transfer equation is

$$T_B = \frac{\alpha}{|\mu|} [\exp(|\mu|L) - 1]. \quad (10)$$

In this case, if $|\mu|L < 1$, we again find $T_B \approx \alpha L$. On the other hand, if $|\mu|L > 1$, the brightness temperature T_B increases exponentially with optical depth. The scale length of the emitting system in an inhomogeneous plasma is

$$L \approx \frac{\Delta\omega}{\omega_{pe}} L_n, \quad (11)$$

(Melrose 1974), where $\Delta\omega/\omega_{pe}$ is the bandwidth to frequency ratio of Langmuir waves. The observed bandwidth to frequency ratio is typically $\Delta\omega/\omega_{pe} \approx 0.1$, as shown in Figure 5a. However, the observed bandwidth is mostly instrumental. It is very difficult to remove the instrumental contribution from the observed bandwidth. Therefore, we theoretically estimate the bandwidth by using the plasma parameters given in Table 1. The Langmuir wave bandwidth $\Delta\omega$ consists of linear and non-linear parts, $\Delta\omega_L + \Delta\omega_{NL}$. The ratio $\Delta\omega_L/\omega_{pe}$ is the relative width of the beam excited Langmuir spectrum, which is given by (Melrose 1980c) $\Delta\omega_L/\omega_{pe} \approx (3v_{Te}^2/2\omega_{pe}^2)k_L \Delta k_L \approx 1.2 \times 10^{-3}$. The spectral broadening $\Delta\omega_{NL}$, which is due to non-linear processes, has three components: $\Delta\omega_{NL} = \Delta\omega_1 + \Delta\omega_2 + \Delta\omega_3$. The first component is due to Doppler broadening caused by random thermal motions of scattering ions and is given by (Melrose 1980c) $\Delta\omega_1/\omega_{pe} = \sqrt{2}v_{Ti}/v_b \approx 1.6 \times 10^{-3}$, where v_{Ti} is the ion thermal speed. The second term $\Delta\omega_2$ is due to wave-wave interactions involving ion acoustic waves and is given by $\Delta\omega_2/\omega_{pe} \approx \omega_s/\omega_{pe} \approx 4 \times 10^{-3}$. The last term $\Delta\omega_3$ is due to strong Langmuir turbulence, which is given by $\Delta\omega_3/\omega_{pe} \approx 1/2 < \delta n_e/n_e > \approx W_L/(2n_e T_e)$, where $< \delta n_e/n_e >$ denotes average density fluctuations due to the formation of cavitons. For typical Langmuir wave energy densities given in Table 3 this yields $\Delta\omega_3/\omega_{pe} \approx 10^{-5}$. Therefore the total intrinsic Langmuir wave bandwidth is given by $\Delta\omega/\omega_{pe} \approx 4 \times 10^{-3}$. This is used to compute the value of L in equation (11).

The scale length of the density variation in the region of Langmuir wave conversion is given by $L_n = |n_e/\nabla n_e|$. In the interplanetary medium, we obtain $L_n = r/2$, assuming $n_e \approx r^{-2}$, where r is the heliocentric distance. From the values given in Table 1, we obtain $L \approx 3 \times 10^{10}$ cm for $r = 1$ AU.

In §§ 4.1–4.4, we calculate both α and μ for each conversion process using the observed Langmuir wave energy densities.

From these values we compute the brightness temperature T_B for electromagnetic waves predicted by each theory. We then compare computed and observed values of type III brightness temperatures to evaluate the feasibility of each conversion mechanism.

4.1. Scattering of Langmuir Waves into Transverse Waves off Thermal Ions ($l + i \rightarrow t + i$)

The emission coefficient α in the case of scattering of Langmuir waves off thermal ions is given by:

$$\alpha = \frac{\pi\omega_{pe}^3 \sin^2 \theta W_L}{6v_g n_e v_{Te}^2 k_L \Delta k_L [1 + (T_e/T_i)]^2}. \quad (12)$$

(see, Tsytovich 1971; Zaitsev 1975). Here W_L is the total energy density of Langmuir waves, T_e and T_i are the electron and ion temperatures, respectively, θ is the angle between the electromagnetic wave vector \mathbf{k} and Langmuir wave vector \mathbf{k}_L , and v_g is the group speed of the electromagnetic waves, given by $v_g = n_i c$, where $n_i \approx 0.5$ for the events of this study. The absorption coefficient μ is given by

$$|\mu| = \frac{m_e}{3m_i T_e} \frac{\pi\omega_{pe}^3 \sin^2 \theta W_L}{6v_g n_e v_{Te}^2 k_L \Delta k_L [1 + (T_e/T_i)]^2}, \quad (13)$$

where m_e and m_i are the electron and ion masses, respectively. For the values of Table 1, and using $\sin^2 \theta = \frac{1}{2}$ (Zaitsev 1975), we obtain:

$$|\mu|L = 6 \times 10^2 \frac{W_L}{n_e T_e}. \quad (14)$$

Even the largest observed value of $W_L/n_e T_e \approx 3 \times 10^{-5}$ (see Table 3) yields $|\mu|L \ll 1$. Therefore, the brightness temperature T_B is determined predominantly by spontaneous scattering:

$$T_B \approx \alpha L, \quad (15)$$

which gives for the above parameters $T_B \approx 0.3f_p^3 W_L/n_e T_e$. We calculate the peak brightness temperature T_B for each type III event using the observed energy densities $W_L/n_e T_e$ from Table 3, and tabulate these in the third column of Table 4.

4.2. Nonlinear Wave-Wave Interactions

Typically the waves involved in any three-wave interaction should satisfy the following energy and momentum conservation conditions:

$$\omega = \omega_L \pm \omega_s; \quad \mathbf{k} = \mathbf{k}_L \pm \mathbf{k}_s, \quad (16)$$

where ω and \mathbf{k} refer to the frequency and wave vector of electromagnetic waves, respectively, and subscripts L and s refer to Langmuir and low-frequency waves (e.g., low-frequency ion-acoustic waves), respectively. The plus (+) corresponds to wave coalescence, e.g., the merging of a Langmuir wave and a low-frequency wave to give an electromagnetic wave ($l + s \rightarrow t$), and the minus (−) corresponds to decay processes, e.g., the decay of a Langmuir wave into a low-frequency wave and an electromagnetic wave ($l \rightarrow t + s$). These processes can be described by the transfer equation (8), where the emission coefficient α and absorption coefficient μ_{\pm} for wave-wave interactions are given by:

$$\alpha = \frac{\kappa}{v_g} \int P_{\pm} T_L T_s \frac{\omega}{\omega_L \omega_s} \frac{d\mathbf{k}_L d\mathbf{k}_s}{h(2\pi)^6}, \quad (17)$$

TABLE 4
MEASURED AND PREDICTED TYPE III BRIGHTNESS TEMPERATURES (T_B) IN (K)

Event (1)	Observed T_B (2)	$l + i \rightarrow t$ (3)	$l + s \rightarrow t$ (4)	$l \rightarrow t + s$ (5)	Strong Turbulence (6)	Direct Coupling (7)
1990 Dec 11	2×10^{12}	1×10^7	8×10^{16}	7×10^{17}	1×10^{14}	7×10^{12}
1990 Dec 23	5×10^{11}
1991 Feb 22	2×10^{11}	3×10^6	6×10^{16}	2×10^{17}	2×10^{13}	2×10^{12}
1991 Mar 7	6×10^{11}	3×10^7	9×10^{16}	1×10^{18}	4×10^{14}	1×10^{13}

NOTE.—Col. (1) gives date of type III event; col. (2), the observed type III brightness temperature T_B ; cols. (3–7), the type III brightness temperature predicted by the four conversion mechanisms; col. (3), spontaneous scattering of Langmuir waves on thermal ions; col. (4), merging of Langmuir and low-frequency waves; col. (5), Langmuir wave decay; col. (6), strong turbulence; and col. (7), direct coupling.

and

$$\mu_{\pm} = \frac{\kappa}{v_g} \int P_{\pm} \left(\frac{T_s}{\omega_s} \pm \frac{T_L}{\omega_L} \right) \frac{dk_L dk_s}{\hbar(2\pi)^6}. \quad (18)$$

Here P_{\pm} is the probability of the wave-wave interaction (Melrose 1980a), and \hbar is the Planck constant. The probability P_{\pm} is given by:

$$P_{\pm} \simeq \sqrt{\frac{m_e}{m_i}} \frac{(2\pi)^5 \hbar e^2 k_s \sin^2 \theta}{8m_e^2 k_L^2 v_{Te}} \delta(k - k_L \pm k_s) \delta(\omega - \omega_L \pm \omega_s). \quad (19)$$

We can integrate equations (17) and (18) using equation (16) and the identity $dk_L = k_L^2 \Delta k_L \Omega_L$, and assuming $k \simeq 0$, $\omega \simeq \omega_L$ and $\omega_s \ll \omega_L$. We also assume $k_s \simeq k_L$ and $\omega_s/k_s \simeq v_{Te} \omega_p/\omega_{pe}$. This gives

$$\alpha \simeq \frac{\kappa e^2 T_L T_s k_L^2 \Delta k_L \sin^2 \theta \Omega_L}{16\pi m_e^2 v_g v_{Te}^2}, \quad (20)$$

and

$$\mu_{\pm} \simeq \frac{\kappa e^2 \omega_s k_L^2 \Delta k_L \sin^2 \theta \Omega_L}{16\pi m_e^2 v_g v_{Te}^2} \left(\frac{T_s}{\omega_s} \pm \frac{T_L}{\omega_L} \right). \quad (21)$$

Using the values of Table 1 and $\sin^2 \theta = \frac{1}{2}$, the optical depth $\mu_{\pm} L$ is:

$$\mu_{\pm} L \simeq 9 \times 10^{-14} \omega_s \left(\frac{T_s}{\omega_s} \pm \frac{T_L}{\omega_L} \right). \quad (22)$$

The low-frequency waves relevant to equation (22) are those which satisfy the conditions of equation (16). These conditions imply that $k_s \simeq k_L$, since $k \simeq 0$ for electromagnetic waves. Using $k_s = 2\pi f_s/c_s$, where f_s is the observed frequency of the high-frequency ion-acoustic waves, $\simeq 3$ kHz, and c_s is the acoustic speed, we find that k_s is about a factor of 100 greater than typical k_L values $\simeq 2.3 \times 10^{-5} \text{ cm}^{-1}$. Even allowing for a Doppler shift of the low-frequency waves due to a solar wind velocity of 400 km s^{-1} , k_s is a factor of 10 larger than k_L . We therefore rule out the high-frequency ion-acoustic waves for any role in the conversion of Langmuir waves by wave-wave interaction.

On the other hand, the low-frequency ion-acoustic waves, i.e., waves below several hundred hertz, could satisfy the conditions of equation (16). However, for the events of the study, there is no observable wave activity at these low frequencies, and therefore we cannot determine T_s from observations. Therefore, we have computed T_s from the threshold value of the WFA receiver, which is $E_s \simeq 2.5 \times 10^{-6} \text{ V m}^{-1}$ at 100 Hz. This gives $T_s \simeq 1.1 \times 10^{14} \text{ K}$ according to equation (7).

We first compute the brightness temperature for the wave merging case. For this case, $\mu_+ > 0$, and therefore equation (9) is used to compute the brightness temperature. Assuming that the low-frequency ion-acoustic waves are near the receiver threshold values, and using even the lowest T_L values in Table 3 ($T_L \simeq 10^{17} \text{ K}$), we obtain $\mu_+ L \gg 1$ from equation (22). Here we have used $\omega_L/2\pi = \omega_{pe}/2\pi \simeq 13 \text{ kHz}$. In these calculations, the non-Doppler shifted frequency of the ion-acoustic waves, $\omega_s/2\pi \simeq 19 \text{ Hz}$ for waves observed at 100 Hz, is used. For $\mu_+ L \gg 1$, equation (9) becomes $T_B = \alpha/\mu_+$. Using equations (20) and (21), this can be expressed as:

$$T_B \simeq \left[T_L T_s / \left(\frac{T_L}{\omega_L} + \frac{T_s}{\omega_s} \right) \omega_s \right]. \quad (23)$$

Assuming that the ion-acoustic waves are at the level of the instrumental threshold, we use equation (23) to calculate T_B due to merging. This value is given in column (4) of Table 4. For $T_s/\omega_s < T_L/\omega_L$, as is the case for our observations, $T_B \simeq T_s \omega_L/\omega_s$. (Note that in eq. [35] of Cairns 1987 the frequency ratio is mistakenly inverted.) For this case, T_B is approximately independent of T_L and depends only on the ion-acoustic wave energy T_s .

In the case of Langmuir wave decay the absorption coefficient μ_- computed from equation (21) is negative, since for our observations $T_s/\omega_s < T_L/\omega_L$. The brightness temperature T_B is then given by equation (10). In this case μ_- leads to an amplification of transverse waves. The main contribution to μ_- is $l \rightarrow t + s$. Substitution of α and μ values into equation (10) gives $T_B \gg T_L$, which is physically unrealistic. In the decay process, saturation occurs when the number of electromagnetic photons equals the number of Langmuir plasmons ($N_t = N_L$), and therefore $T_B = T_L$. Clearly, the amount of electromagnetic energy cannot exceed the energy of the pump Langmuir waves. It also follows that for saturation, the number of phonons N_s generated by this process equals the number of Langmuir plasmons, and therefore $N_L \simeq N_s$. (Note that it is incorrectly stated in Cairns 1987 that $N_s \gg N_L$ at saturation.) In column (5) of Table 4 we give the values for T_B assuming the decay process has saturated, and therefore the T_B values are just the measured T_L values obtained from Table 3. We note, however, that the lack of observable ion-acoustic activity in our data may indicate that the decay process has not saturated, in which case we should have $N_t \simeq N_s$, yielding $T_B \simeq T_s \omega_L/\omega_s$. This would give T_B values found previously for the merging case, i.e., the values in column (4) of Table 4.

4.3. Strong Langmuir Turbulence

The time scales of the Langmuir spikes seen in the FES data of the December 11 and March 7 events (Fig. 3 and 11) are of

the order of 1 msec (similar examples are shown by Kellogg et al. 1992; Gurnett et al. 1993). By taking the solar wind velocity as 400 km s^{-1} in the radial direction, one obtains 400 m as the radial spatial scale (l_{\parallel}). The Debye length (λ_D) on these days was approximately 20 m. The typical spatial scale size of the Langmuir wave collapse (l_0) is approximately equal to $20\lambda_D$ (Papadopoulos et al. 1974). Thus the observed spatial scale satisfies $l_{\parallel} \leq l_0$, suggesting that strong turbulence phenomena may indeed occur during these events.

If strong turbulence effects, such as modulational instability and spatial collapse or self-focusing of Langmuir waves, are important, the relative level of Langmuir waves $W_L/n_e T_e$ should exceed the threshold value for strong turbulence, which is given by (Goldman & Nicholson 1978):

$$\frac{W_{\text{th}}}{n_e T_e} = 24(\Delta k_0 \lambda_D)^2. \quad (24)$$

Here Δk_0 is the half-width of an assumed spherically symmetric Langmuir wave packet. We use the formula given by Melrose & Goldman (1987):

$$\frac{\Delta k_0}{k_0} = \frac{\Delta v_b}{v_b \pi \sqrt{N}}, \quad (25)$$

where $k_0 = k_L$, and N is the number of linear growth times before the onset of modulational instability. As seen in the FES events in Figures 3, 9, and 11, the ratio of the peak to background Langmuir intensities is $\approx 10^3$, giving $N \approx 7$. For $\Delta v_b/v_b \approx 0.15$ and $k_0 \approx k_L \approx 2.3 \times 10^{-5} \text{ cm}^{-1}$, we obtain $\Delta k_0 \approx 0.02k_0$. Using this and other values from Table 1, we obtain from equation (24) the threshold energy density $W_{\text{th}}/n_e T_e \approx 2 \times 10^{-5}$. We see from Table 3 that the observed Langmuir wave energy densities are close to the threshold energy density. Indeed, for the two events which display millisecond spikes (December 11 and March 7), the measured wave amplitudes appear to exceed the threshold energy. The millisecond spikes have energy densities of approximately 2×10^{-4} , clearly exceeding the threshold energy density by one order of magnitude. It should be noted that equation (24) is appropriate as long as the threshold value for modulational instability obtained from this expression is less than threshold values for electrostatic and electromagnetic decay instabilities. If this is not the case, then the waves can scatter out of resonance with the beam before Δk_0 becomes small enough for equation (24) to apply. In such a situation, strong turbulence may be more likely to occur via a backscatter into a weak turbulence condensate. However, in the present case, there is no observable low frequency ion-acoustic wave activity and it appears that the decay instabilities are not operating with their maximum efficiency. Therefore equation (24) is still appropriate for estimating the threshold values. Thus both the small spatial scales of the Langmuir spikes and the high-energy densities of the Langmuir waves suggest the presence of Langmuir solitons during these two events. Moreover, in the determination of the bandwidth to frequency ratio of Langmuir waves (§ 4), we found that the observed values (≈ 0.1) far exceeded the ratios expected from the Langmuir dispersion relation ($\approx 1.2 \times 10^{-3}$). As noted in § 4, the wide bandwidth of the observed waves is mainly instrumental. However, a considerable part of the observed bandwidth may be due to nonlinear processes, such as nonlinear wave-wave interactions and strong turbulence processes.

The Zakharov equations describing strong Langmuir turbulence excited by electron beams show that the main energy-containing region of Langmuir turbulence is the long-wavelength region of the source rather than the collapsed wave packets (see Galeev et al. 1977; Kruchina et al. 1980). The generation of electromagnetic waves is assumed due to the scattering of the long-wavelength Langmuir turbulence on the random distribution of collapsed cavitons. The emissivity of the electromagnetic waves is given by:

$$\frac{dW_T}{dt} = \beta \frac{\omega_{pe} W_L^2}{4n_e T_e} \left(\frac{3T_e}{m_e c^2} \right)^{3/2} \quad (26)$$

(Kruchina et al. 1980), where W_L is the total energy density in the long-wavelength Langmuir waves. The constant β is approximately 0.3 (Galeev et al. 1977), and it reflects the fact that only a fraction of Langmuir wave energy is contained in collapsed wave packets (see Appendix).

A derivation of this equation may be found in the Appendix. This equation is similar to the transfer equation (8), where the induced effects are assumed not to be important ($\mu \approx 0$). The emission coefficient α in the present case can be written as $\alpha \approx \beta(f_{pe} W_L^2 c^2)/(4\kappa^2 n_e T_e n_i^2 f^2 \Delta f)(3\kappa T_e/m_e c^2)^{3/2}$ by using equations (1), (8), and (26). Here we have assumed that $\Delta t \approx L/v_g$, $k \approx 2\pi f/c$ and $\Delta k \approx 2\pi \Delta f/v_g$, $f_{pe} \approx f$, and $\Omega_i \approx 2\pi$. This yields $T_B = 2 \times 10^{38} f_{pe}(W_L/n_e T_e)(W_L/f^2 n_i^2)$. We assume that the observed Langmuir wave energy densities given in Table 3 represent the total energy density W_L . We calculate the expected brightness temperatures of the electromagnetic emission due to strong Langmuir turbulence and tabulate them in column (6) of Table 4.

4.4. Direct Coupling

The Langmuir and electromagnetic waves propagate independently in a weakly inhomogeneous plasma if the geometrical optics approximation ($d\epsilon/dz)\lambda/2\pi \ll \epsilon$ is valid everywhere, where ϵ is the dielectric permittivity, λ is the wavelength, and z is the coordinate along which the density is varying. However, if the waves pass through regions where the geometrical optics approximation is not valid (for example, interaction regions where the refractive index $n \approx 0$), they no longer remain independent but are coupled, i.e., their amplitudes bear a specific relationship to one another. This phenomenon is called direct coupling, and in the present case involves the partial conversion of Langmuir wave energy into electromagnetic wave energy.

In the solar corona or in the interplanetary medium, where the electron density is decreasing radially outward, Langmuir waves propagating toward the region of increasing density (i.e., towards the Sun) encounter coupling regions where $\omega \approx \omega_{pe}$, i.e., regions where their refractive index $n_L \approx 0$. (Beam-excited Langmuir waves have wave vectors directed away from the sun; however, induced scattering by thermal ions is expected to produce oppositely directed Langmuir waves. Such a secondary Langmuir spectrum is a requirement for the generation of second harmonic type III emission [Zheleznyakov 1977] as well as for the occurrence of the direct coupling mechanism.) In such a coupling region, the Langmuir wave is reflected back and partially converted into an electromagnetic wave, and both waves propagate in the direction of decreasing density, i.e., toward greater heliocentric distance. Physically, the reason for the coupling is that the inward propagating Langmuir waves are refracted by the density gradient, producing a bending of the lines of force and thus a curl in the electric field

$\nabla \times E$ (Field 1956). Thus a fraction of Langmuir wave energy gets converted into escaping electromagnetic radiation at ω_{pe} . Such direct coupling has been suggested as a possible mechanism for fundamental plasma emission (Ginzburg & Zheleznyakov 1958). Field (1956) has suggested that the coupling of Langmuir waves with electromagnetic waves can also take place if the Langmuir wave encounters sharp boundaries such as shock fronts, i.e., if $l \ll \lambda_L$ is satisfied, where l is the spatial scale of the density jump and λ_L is the Langmuir wavelength.

In a smoothly varying isotropic plasma where the ambient magnetic field is neglected, Zheleznyakov (1970) has shown that the efficiency of conversion is maximum at an optimum angle ϕ_{opt} between the Langmuir wave vector and density gradient and is given by:

$$\sin \phi_{opt} \simeq \frac{v_{ph}}{c} \left(\frac{3c}{2\omega_{pe} L_n} \right)^{1/3},$$

where v_{ph} is the phase velocity of Langmuir waves. For small angles, one can write $\sin \phi_{opt} \simeq \phi_{opt}$. If the Langmuir waves have a broad angular spectrum, only those waves for which the angle $\phi \leq \phi_{opt}$ can effectively get converted into electromagnetic emission. The mean conversion efficiency Q_D is given by:

$$Q_D = \frac{\pi}{4\Omega_L} \phi_{opt}^2. \quad (27)$$

(Zheleznyakov 1970). This gives a value of $\simeq 6.3 \times 10^{-8}$ for Q_D for typical values given in Table 1.

For the magnetized case, the efficiency of conversion of Langmuir waves into escaping ordinary waves is given by:

$$Q_D = \frac{v_{ph}^2}{c\omega_{pe} L_n \Omega_L} \left(\frac{\omega_{pe} + \omega_B}{\omega_B} \right)^{1/2}. \quad (28)$$

(Zheleznyakov 1970; Melrose 1980b), where ω_B is the electron cyclotron frequency. (Note that equation [28] cannot be reduced to equation [27] for the case of $\omega_B = 0$, since the equations are derived using different approximations.) For typical values given in Table 1, we obtain $Q_D \simeq 3.4 \times 10^{-9}$. This equation is valid only if the following inequality is satisfied:

$$\omega_B/\omega > (c/\omega L_n)^{2/3}, \quad (29)$$

(Zheleznyakov 1970), as is the case for typical solar wind conditions.

In the presence of a magnetic field, the electromagnetic wave is split into two modes called ordinary (*o*-mode) and extraordinary (*x*-mode) waves, with refractive indices n_o and n_x , respectively. The refractive index n_x of the *x*-wave is zero at the layer where $(\omega_{pe}/\omega)^2 \simeq 1 - \omega_B/\omega$, whereas both n_o and n_L are zero in the plasma layer $\omega \simeq \omega_{pe}$. Thus the $n_x \simeq 0$ layer lies at greater heliocentric distance than the $n_L \simeq 0$ ($\omega \simeq \omega_{pe}$) layer. If the distance between these two layers z is greater than the wavelength of the extraordinary wave (λ_x), the *x*-wave cannot escape from the coupling region where $n_L \simeq 0$. However, if the magnetic field is very weak, or the gradient in the density is very steep, so that in the interaction region the condition of equation (29) is not satisfied, then $\lambda_x > z$. Consequently, the *x*-wave will be only weakly damped in the coupling region, and even though $n_x^2 < 0$ in this region, it will be able to propagate outward through the solar wind. This case (weak field or steep density gradient) is equivalent to the case of the isotropic plasma discussed earlier, where the conversion efficiency Q_D is given by equation (27) rather than equation (28).

For typical solar wind magnetic field strengths and density gradients, condition (29) is satisfied. (This condition may not be satisfied for fields less than about 0.01γ or for sharp discontinuities, such as shock fronts.) Consequently, for typical solar wind conditions, only ordinary electromagnetic radiation may escape from the interaction region and propagate freely outward in the solar wind. In this case the extraordinary component is strongly damped in the interaction region and cannot propagate outward through the $n_x^2 \simeq 0$ layer.

Usually the efficiency of conversion Q_D is defined as the ratio of the electromagnetic wave flux to Langmuir wave flux. In terms of effective temperatures, one can write:

$$T_B = \frac{n_L^2 \Omega_L}{n_i^2 \Omega_i} Q_D T_L, \quad (30)$$

where n_L and n_i are the refractive indices of Langmuir and electromagnetic waves, respectively, and $n_L^2/n_i^2 \simeq c^2/3v_{Te}^2$. For $\Omega_i \simeq 2\pi$ and $\Omega_L \simeq 0.6\pi$, we obtain:

$$T_B \simeq \frac{cv_{ph}^2}{6\pi v_{Te}^2 \omega_{pe} L_n} \left(\frac{\omega_{pe} + \omega_B}{\omega_B} \right)^{1/2} T_L. \quad (31)$$

This equation is similar to a solution to transfer equation (8), where the induced effects are neglected ($\mu \simeq 0$). The emission coefficient α in the present case $\alpha \simeq (cv_{ph}^2)/(6\pi v_{Te}^2 \omega_{pe} L_n L) [(\omega_{pe} + \omega_B)/\omega_B]^{1/2} T_L$. This can be written as $T_B \simeq 1 \times 10^{-2} [(\omega_{pe} + \omega_B)/\omega_B]^{1/2} T_L/f_{pe}$. The cyclotron frequency $\omega_B/2\pi$ is taken to be 140 Hz. Using the observed T_L values in Table 3, the brightness temperatures of the electromagnetic emission predicted by the direct coupling theory are listed in column (7) of Table 4. For this calculation we are addressing only the case of an idealized smoothly varying electron density distribution without including small scale electron density inhomogeneities.

5. DISCUSSION

The first Langmuir wave conversion mechanism which we have evaluated in this study is scattering of Langmuir waves by thermal ions (§ 4.1). This conversion mechanism does not appear to be of importance for the generation of the interplanetary type III bursts of this study beyond 1 AU. We have shown in § 4.1 that even using the most intense Langmuir signals observed for these events, the optical depth for induced scattering is $\mu L \ll 1$, ruling out the possibility of induced scattering playing any role in conversion processes. This implies that if the scattering on thermal ions is important for conversion, only spontaneous scattering plays a role. However, the expected brightness temperatures due to spontaneous scattering are too low in comparison with observed values [as seen by comparing column (3) with column (2) in Table 4], even though peak Langmuir wave intensities were used in the calculation. Thus, neither induced nor spontaneous scattering mechanisms seem to play a significant role in converting Langmuir waves into fundamental type III emission in the interplanetary medium. The scattering mechanism has widely been believed to be responsible for metric type III bursts, which arise in the solar corona. Clearly, Langmuir wave energy densities in coronal source regions cannot be observed; thus, this mechanism cannot be directly tested for metric type III bursts. However, if type III bursts in both the corona and interplanetary space are generated by the same mechanism, our results would not support scattering as an important conversion mechanism for type III bursts.

The second conversion mechanism which has been invoked mainly for interplanetary type III bursts involves wave-wave interactions. Low frequency ion-acoustic waves in the frequency range around 100 Hz satisfy the conservation conditions in equation (16), and are likely to be involved in wave-wave interactions, as suggested by Lin et al. (1986). However, no wave activity in either electric field or magnetic field measurements has been observed by the URAP experiment in this frequency range in association with type III bursts. The low-frequency ion-acoustic waves observed by Lin et al. had energy densities of approximately $E_s \approx 40 \times 10^{-6} \text{ V m}^{-1}$. Assuming that the level of low-frequency ion-acoustic waves for our events is near the WFA threshold value of $E_s \approx 2.5 \times 10^{-6} \text{ V m}^{-1}$, we have calculated the expected peak brightness temperatures for wave-wave interactions. The analysis in § 4.2 has shown that for the process of the merging of Langmuir and low-frequency waves the computed values of T_B are approximately a factor of 10 less than the observed values of T_L . For the case of Langmuir wave decay, however, we take the brightness temperatures to be equal to T_L , assuming that the decay process is saturated. Values of T_B are given in column (4) of Table 4 for the case of wave merging and in column (5) for the case of wave decay. These values are four to six orders of magnitude more than the observed values of T_B . For wave merging to be a feasible conversion mechanism, levels of low-frequency waves far below those observed by Lin et al. (1986) would have to be present. In addition, if these merging and decay processes do generate electromagnetic waves with the high efficiencies suggested in this analysis, a mechanism is needed for reducing the electromagnetic wave amplitudes to the relatively low levels observed.

A further difficulty with the Langmuir wave decay mechanism is the following. The observed peak energy densities of the Langmuir waves (Table 3) exceed the threshold energy densities for the electrostatic decay instability ($l \rightarrow l + s$) and the electromagnetic decay instability ($l \rightarrow t + s$). The threshold energy density for the electrostatic decay instability is given by $4(\Gamma_s \Gamma_l / \omega_s) \omega_{pe} \approx 2.5 \times 10^{-5}$, whereas the threshold energy density for the electromagnetic decay instability is given by $\approx 4(\Gamma_s \Gamma_l / \omega_s) \omega_{pe} \approx 10^{-11}$ (Lin et al. 1986), where Γ_s , Γ_l , and Γ_t are the damping rates for the ion-acoustic, Langmuir, and electromagnetic waves, respectively. Therefore, if the decay instabilities are playing any role in the source regions of Langmuir waves, the number of ion-acoustic phonons should be approximately equal to those of Langmuir waves. This implies that the electric field of ion-acoustic waves is given by $E_s \approx E_L (m_e/m_i)^{1/4} (k_s/\lambda_D)^{3/2} [(k_s/k_L)^3 (\Omega_s/\Omega_L)]^{1/2}$. For the electrostatic decay instability, using $k_s \approx 2k_L$, $\Delta k_s \approx \Delta k_L$, and $\Omega_s \approx 4\Omega_L$, we obtain $E_s \approx 0.025 E_L$, using values in Table 1. For the electromagnetic decay instability, if we take $k_s \approx k_L$, $\Delta k_s \approx \Delta k_L$, and $\Omega_s \approx \Omega_L$, we obtain $E_s \approx 1.6 \times 10^{-3} E_L$. The peak electric fields of the Langmuir waves E_L , as seen in Table 3, range from approximately 2–13 mV m⁻¹. Therefore, the range in expected E_s values is approximately equal to 6×10^{-6} – $32 \times 10^{-6} \text{ V m}^{-1}$ in the case of the electrostatic decay instability, and 4×10^{-6} – $32 \times 10^{-6} \text{ V m}^{-1}$ in the case of the electromagnetic decay instability. These values are consistent with the value of E_s of about $40 \times 10^{-6} \text{ V m}^{-1}$ reported by Lin et al. (1986) for the event of 1979 March 11. However, below 500 Hz we do not observe any wave activity above the instrumental threshold value of $2.5 \times 10^{-6} \text{ V m}^{-1}$. Therefore, the level of low-frequency waves predicted by both decay instabilities is substantially greater than the maximum wave amplitudes possible

from our observations. The absence of observed low-frequency ion-acoustic waves indicates that either 1) the electrostatic and electromagnetic decay instabilities are completely suppressed by some unknown mechanism or 2) the decay processes are operating below their maximum efficiency, producing the daughter ion-acoustic waves below instrumental threshold levels. The discrepancy between the observation of significant ion-acoustic wave activity by Lin et al. (1986) and the absence of observed ion acoustic waves in our study is difficult to explain. We note that Gurnett et al. (1993) also did not observe ion-acoustic waves associated with type III related Langmuir waves.

The third mechanism considered in the current study is electromagnetic emission at ω_{pe} by strongly turbulent Langmuir waves (§ 4.3). The conversion of Langmuir waves due to scattering on collapsed cavitons gives predicted brightness temperatures shown in column (6) of Table 4. These are about two orders of magnitude greater than the observed values, which gives better agreement with observations than either wave-particle or wave-wave mechanisms discussed earlier. We have found evidence of small spatial scales and field strengths exceeding thresholds for modulational instability for some of our events, suggesting the presence of strong turbulence effects. However, the lack of simultaneous observable signals at about 2 Hz and 100 Hz (see Figs. 1, 7, 8, and 10), which should be excited due to modulational and decay instabilities, respectively, poses some questions about the role of strong turbulence in conversion processes. It is, however, possible that the signals at these frequencies are below the instrumental threshold values, making it difficult to observe the wave activity. We are examining other intense Langmuir events observed by the URAP experiment for any possible correlation with low-frequency waves as well as calculating the predicted wave levels of the low frequency waves by the oscillating two-stream or modulational instabilities.

Goldman et al. (1980) have calculated the emission from a single collapsing (self-similar) wave packet which occurs when small spatial scales are reached. However, as pointed out by Kruchina et al. (1980), the fundamental radiation produced by such a coherent process is negligible because most of the Langmuir energy is in the long-wavelength region of the source. In addition, the turbulence is almost isotropic in the short-wavelength region, and the average electromagnetic field $E_T \approx \langle \delta n_e E_L \rangle$ is close to zero. Therefore, Langmuir conversion from the collapsing wave packets themselves (as opposed to the mechanism of scattering on collapsed cavitons, discussed above) does not appear capable of producing significant electromagnetic emission.

Finally, regarding the direct coupling of Langmuir with electromagnetic waves during their propagation in an inhomogeneous plasma, Ginzburg & Zheleznyakov (1958) noted that this process can be as efficient as spontaneous scattering in the coronal plasma. Indeed, as seen in column (7) of Table 4, the brightness temperatures predicted by the direct coupling process exceed the observed T_B values by one order of magnitude or less. These are closer to observed values than those computed from the other mechanisms. Therefore, direct coupling is clearly a viable conversion mechanism for fundamental type III emission in the interplanetary medium. However, one should note that the coronal and interplanetary plasma is known to consist of large- as well as small-scale density structures, and, in the presence of sharp discontinuities in the density, Field (1956) has shown that the conversion of Lang-

muir waves into transverse waves can be even more efficient than in the smoothly varying density gradient considered in the current study.

The efficiency of conversion Q_R due to spontaneous scattering is $Q_R = (\omega_{pe}^4 L) / (12\pi n_e c^3 v_{Te})$ (Zheleznyakov 1970). For solar wind conditions this yields $Q_R \simeq 3.5 \times 10^{-12}$, using the values of Table 1. The mean conversion efficiency due to direct coupling in a smoothly varying magnetized plasma, using equation (28), is $Q_D \simeq 3.4 \times 10^{-9}$, thereby exceeding Q_R by several orders of magnitude for typical conditions in the interplanetary medium. We have seen from Table 4 that direct coupling is a far more efficient mechanism than spontaneous scattering in the interplanetary medium. It is also important to note that the efficiency of spontaneous scattering is about equal to that of direct coupling, $Q_R \simeq Q_D$, in the region of the solar corona where meter wavelength type III bursts are generated (Ginzburg & Zheleznyakov 1958). Thus, if a single conversion mechanism is responsible for fundamental type III emission in both the corona and the interplanetary medium, the most likely mechanism is the direct coupling mechanism.

It seems clear from these results that the Langmuir wave scattering on thermal ions is not a viable conversion mechanism, since it predicts T_b at least three orders of magnitude below observed values. The remaining three mechanisms, however, predict brightness temperatures in excess of observations. This analysis has assumed spatial homogeneity, implying, for instance, that Langmuir wave field strengths used for the computations occur throughout the source region. Langmuir waves, however, obviously occur in bursts; therefore, peak field amplitudes are not characteristic of the entire source region. Therefore, lower levels of Langmuir waves may also play a role in electromagnetic wave generation, thereby reducing type III brightness temperatures below levels predicted in Table 4.

It is also possible that some process reduces the observed radiation below levels produced by the conversion mechanisms. The scattering and absorption of radiation near the plasma frequency by ambient density fluctuations in the source region are the most likely causes of depressing the emitted radiation. Thejappa & Kundu (1992) have used a ray tracing technique to predict the change in brightness temperatures due to refraction, absorption, and scattering by density fluctuations in the solar corona. They have demonstrated that to reduce the brightness temperature by about one order of magnitude, a level of density fluctuations $\Delta n_e/n_e \simeq 0.14$ would be required. It is unclear whether such effects can reduce brightness temperatures by many orders of magnitude, which would seem to be required to make wave-wave interactions a viable conversion mechanism.

6. SUMMARY AND CONCLUSIONS

In this study we have presented the first observational tests of possible mechanisms for converting Langmuir waves into electromagnetic radiation at the fundamental of the plasma frequency ω_{pe} . The data used for evaluating these conversion theories are the *Ulysses* URAP observations of three interplanetary

type III radio bursts with emission at ω_{pe} and for which simultaneous Langmuir wave activity occurs. The major results of this study are as follows.

1. The scattering of Langmuir waves by thermal ions does not appear to be of importance in the conversion process. Induced scattering is optically thin, even for the most intense Langmuir bursts. The scattering of Langmuir waves would therefore be due predominantly to spontaneous processes. However, the brightness temperatures of electromagnetic waves predicted by the spontaneous scattering mechanism are smaller than observed type III brightness temperatures by approximately five orders of magnitude. This suggests that scattering processes are unlikely to play a significant role in the conversion process.

2. Although low-frequency waves are necessary for the conversion of Langmuir waves through wave-wave interactions, no low-frequency waves have been observed for the events of this study. Using receiver threshold values for the low-frequency wave amplitudes, brightness temperatures computed from the wave-wave conversion process are significantly greater, by four to six orders of magnitude, than the observed type III brightness temperatures. From our observations it is clear that if the electromagnetic decay instability is the dominant conversion mechanism, it is operating with far less efficiency than in the cases reported by Lin et al. (1986).

3. The short durations of observed Langmuir spikes, the large energy densities of the observed Langmuir waves, and the broad bandwidth of the waves relative to that expected from the Langmuir dispersion relation suggest that strong turbulence effects are important in the interplanetary medium and thus may play a role in Langmuir wave conversion processes. The brightness temperatures predicted from the scattering of long wavelength Langmuir waves on collapsed Langmuir cavitons are higher than observed values by approximately two orders of magnitude, indicating that this is a viable conversion mechanism for type III bursts.

4. The direct coupling of Langmuir waves with electromagnetic waves due to wave propagation in a smoothly varying plasma yields predicted brightness temperatures which are greater than observed values by one order of magnitude or less. Therefore, direct coupling clearly is a viable mechanism for Langmuir wave conversion.

From our comparison of observed type III brightness temperatures with values predicted by four conversion mechanisms, it appears that the strong turbulence and the direct coupling mechanisms are the most feasible processes for generating interplanetary type III radio bursts.

We thank V. V. Zheleznyakov, M. J. Reiner, P. Chaturvedi, and the referee for their helpful comments on the manuscript and R. J. Macdowall for discussions regarding URAP data. We especially wish to thank P. Kellogg for invaluable contributions which made this study possible. The research of G. T. and D. L.-F. is supported by NASA grant NAG 5-1134.

APPENDIX

In the strong turbulence limit, the main energy-containing region of the Langmuir spectrum is the long wavelength region where the primary pumping of energy into Langmuir waves takes place (Galeev et al. 1977; Kruchina et al. 1980). The cavitons with trapped intense Langmuir oscillations arise mainly in this region. The numerical solutions of the Zakharov equations (Nicholson et al. 1978; Hafizi et al. 1982; Robinson & Newman 1989) where an electron-beam driver is included exhibit a (short) "cascade" from

beam-resonant Langmuir modes down to long-wavelength “condensate.” Most of the spectral energy is in the long wavelength condensate. The condensate can give rise to the observed intensities of electromagnetic emission both at ω_{pe} and $2\omega_{pe}$. The characteristic scale lengths in this region correspond to the threshold of the modulational instability, $k_0 \simeq 1/\lambda_D \sqrt{W_L/(3n_e T_e)}$. The conversion of Langmuir waves into electromagnetic waves is associated with the fact that long-wavelength plasmons originating from the source region mix their phases due to scattering on the density fluctuations in the cavities. The characteristic time of phase mixing is determined by the effective scattering frequency, $\nu_{cor} \simeq v_g/l_0$, where $v_g = 3k_L \lambda_D^2 \omega_{pe}$ is the group velocity of Langmuir waves, and $l_0 \simeq 1/k_0$ is the distance between the cavities. Thus, $\nu_{cor} \simeq 3k_L^2 \lambda_D^2 \omega_{pe} \simeq \omega_{pe} W_L/(n_e T_e)$. The equation describing the conversion of long-wavelength plasmons into electromagnetic waves is described in the present case by:

$$-\frac{2i}{\omega_{pe}} \frac{\partial \mathbf{E}_t}{\partial t} + \frac{c^2}{\omega_{pe}^2} \nabla \times \nabla \times \mathbf{E}_t + \frac{\delta n_e}{n_e} \mathbf{E}_L = 0. \quad (A1)$$

Here \mathbf{E}_t and \mathbf{E}_L are the complex amplitudes of the transverse (electromagnetic) and longitudinal (Langmuir) components of the electric field, respectively. There was a typographical error in equation (1) of Kruchina et al. (1980), which has been corrected here. By using the Fourier series expansions for the electric field amplitudes in equation (A1) and averaging over the random phases of Langmuir waves, one obtains the rate equation:

$$\sum_{\mathbf{k}} \frac{dE_t^2}{dt} \simeq \frac{\omega_{pe}^2}{2\nu_{cor}} \sum_{\mathbf{k}} \sum_{\mathbf{k}_L} \left(\frac{\delta n_{\mathbf{k}-\mathbf{k}_L}}{n_e} \right)^2 |E_{\mathbf{k}_L}|^2 \sin^2 \theta, \quad (A2)$$

(Kruchina et al. 1980; Shapiro & Shevchenko 1984), where θ is the angle between the wave vectors \mathbf{k} and \mathbf{k}_L . The equation (A2) can be written in terms of total energy densities of electromagnetic and Langmuir wave as:

$$\frac{dW_T}{dt} = \frac{\omega_{pe}}{4\nu_{cor}} \left(\frac{\langle \delta n_e \rangle}{n_e} \right)^2 W_L \left(\frac{3T_e}{m_e c^2} \right)^{3/2}. \quad (A3)$$

Here the following relations are used: $W_T = \sum_{\mathbf{k}} E_{\mathbf{k}}^2/4\pi$, $(\langle \delta n_e \rangle/n_e)^2 W_L = \sum_{\mathbf{k}} \sum_{\mathbf{k}_L} (\delta n_{\mathbf{k}-\mathbf{k}_L}/n_e)^2 E_{\mathbf{k}_L}^2/4\pi$. The average density fluctuations in density cavities are related to the energy density of long-wave Langmuir waves as $\langle \delta n_e/n_e \rangle^2 \simeq \beta [W_L/(n_e T_e)]$, where $\beta \simeq 0.3$ is the fraction of Langmuir wave energy in Langmuir solitons (Galeev et al. 1977). By substituting $\nu_{cor} \simeq \omega_{pe} W_L/n_e T_e$ in equation (A3), we obtain the equation given in Kruchina et al. (1980) for the emissivity of electromagnetic waves:

$$\frac{dW_T}{dt} = \beta \frac{\omega_{pe} W_L^2}{4n_e T_e} \left(\frac{3T_e}{m_e c^2} \right)^{3/2}. \quad (A4)$$

REFERENCES

- Cairns, I. H. 1987, *J. Plasma Phys.*, 38, 169
Dulk, G. A., Steinberg, J. L., & Hoang, S. 1984, *A&A*, 141, 30
Fainberg, J., Evans, L. G., & Stone, R. G. 1972, *Science*, 178, 743
Fainberg, J., & Stone, R. G. 1974, *Space Sci. Rev.*, 16, 145
Field, G. B. 1956, *ApJ*, 124, 555
Galeev, A. A., Sagdeev, R. Z., Shapiro, V. D., & Shevchenko, V. I. 1977, *Soviet Phys.-JETP Lett.* 46, 711
Ginzburg, V. L., & Zheleznyakov, V. V. 1958, *Soviet Astron.-AJ*, 2, 653
Goldman, M. V., & Nicholson, D. R. 1978, *Phys. Rev. Lett.*, 41, 406
Goldman, M. V., Reiter, F. G., & Nicholson, D. R. 1980, *Phys. Fluids*, 23, 388
Gurnett, D. A., Anderson, R. R., & Tokar, R. L. 1980, in *IAU Symp. 86, Radio Physics of the Sun*, ed. M. R. Kundu & T. E. Gergely (Dordrecht: Reidel), 369
Gurnett, D. A., & Frank, L. A. 1978, *J. Geophys. Res.*, 83, 58
Gurnett, D. A., Hospodarsky, G. B., Kurth, W. S., Williams, D. J., & Bolton, S. J. 1993, *J. Geophys. Res.* 98, 5631
Hafizi, B. J., Weatherall, J. C., Goldman, M. V., & Nicholson, D. R. 1982, *Phys. Fluids* 25, 392
Kellogg, P. J. 1986, *A&A*, 169, 329
Kellogg, P. J., Goetz, K., Howard, R. L., & Monson, S. J. 1992, *Geophys. Res. Lett.*, 19, 1303
Kruchina, E. N., Sagdeev, R. Z., & Shapiro, V. D. 1980, *Soviet Phys.-JETP Lett.*, 32, 419
Lin, R. P., Levedahl, W. K., Lotko, W., Gurnett, D. A., & Scarf, F. L. 1986, *ApJ*, 308, 954
Melrose, D. B. 1974, *Sol. Phys.*, 35, 441
———. 1977, *Radiophys. and Quantum Electron.*, 20, 945
———. 1980a, *Space Sci. Rev.*, 26, 3
———. 1980b, *Australian J. Phys.*, 33, 121
———. 1980c, *Plasma Astrophysics*, Vol. 2 (New York: Gordon & Breach)
Melrose, D. B. 1986, *Instabilities in Space and Laboratory Plasmas* (Cambridge: Cambridge Univ. Press)
———. 1989, *Sol. Phys.*, 120, 369
Melrose, D. B., Dulk, G. A., & Cairns, H. I. 1986, *A&A*, 163, 229
Melrose, D. B., & Goldman, M. V. 1987, *Sol. Phys.*, 107, 329
Nicholson, D. R., Goldman, M. V., Hoyng, P., & Weatherall, J. 1978, *ApJ*, 223, 605
Papadopoulos, K., Goldstein, M. L., & Smith, R. A. 1974, *ApJ*, 190, 175
Reiner, M. J., Fainberg, J., & Stone, R. G. 1992, *ApJ*, 394, 340
Robinson, P. A., & Newman, D. L. 1989, *Phys. Fluids*, 1, 2319
Shapiro, V. D., & Shevchenko, V. I. 1984, in *Handbook of Plasma Physics*, ed. M. N. Rosenbluth & R. Z. Sagdeev (New York: Elsevier Science Publ.), 123
Smith, D. F. 1970, *Adv. Astron. Astrophys.*, 7, 147
———. 1977, *ApJ*, 216, L53
Steinberg, J. L., Dulk, G. A., Hoang, S., Lecacheux, A., & Aubier, M. G. 1984, *A&A*, 140, 39
Steinberg, J. L., & Hoang, S. 1986, *Ann. Geophys.*, 4, 429
Steinberg, J. L., Hoang, S., & Dulk, G. A. 1985, *A&A*, 150, 205
Stone, R. G., et al. 1992, *A&AS*, 92, 291
Takakura, T. 1979, *Sol. Phys.*, 62, 375
Thejappa, G., & Kundu, M. R. 1992, *Sol. Phys.*, 140, 19
Tokar, R. L., & Gurnett, D. 1980, *J. Geophys. Res.*, 85, 2353
Tsytoich, V. N. 1971, *Theory of Turbulent Plasma* (Moscow: Atomizdat)
Zaitsev, V. V. 1975, *Soviet Astron. Lett.*, 5, 206
———. 1977, *Radiophys. Quantum Electron.*, 20, 951
Zheleznyakov, V. V. 1970, *Radio Emission of the Sun and Planets* (New York: Pergamon)
———. 1977, *Electromagnetic Waves in Space Plasmas: Generation and Propagation* (Moscow: Nauka)